applied sciences

MDPI

Article

MgO Dispersed on Activated Carbon as Water Tolerant Catalyst for the Conversion of Ethanol into Butanol

Stefano Cimino, Jessica Apuzzo and Luciana Lisi *

Instituto di Ricerche sulla Combustione-CNR, Piazzale Tecchio 80, 80125 Naples, Italy; stefano.cimino@cnr.it (S.C.); j.apuzzo@irc.cnr.it (J.A.)

* Correspondence: luciana.lisi@cnr.it

Received: 4 March 2019; Accepted: 27 March 2019; Published: 1 April 2019

Abstract: MgO supported on activated carbon (AC) with a load ranging from 10% to 30% has been investigated as catalyst for the conversion of ethanol into butanol at 400 °C in a fixed bed reactor at different GHSV. Catalysts have been characterized by XRD, SEM/EDX, and N_2 physisorption at 77 K. The high dispersion of MgO into the pores of the support provides strongly enhanced performance with respect to bulk MgO. MgO/AC catalysts have been also tested under wet feed conditions showing high water tolerance and significantly larger butanol yield with respect to an alumina supported Ru/MgO catalyst. After wet operation, the increased surface area of the catalyst leads to better performance once dry feed conditions are restored.

Keywords: bio-ethanol; butanol; Guerbet reaction; catalyst; supported MgO; activated carbon

1. Introduction

The conversion of bio-ethanol to butanol as additive for gasoline has been recently investigated in order to upgrade one of the products of (Acetone Butanol Ethanol) ABE fermentation of biomass into a higher fuel-soluble alcohol with a greater calorific value [1]. Coupling of ethanol takes place according to the Guerbet reaction, generally through a catalytic pathway [2]. Catalysts proposed for the Guerbet reaction are supported metals (Ru, Rh, Pd, Pt, Au, Ni, Ag), hydroxyapatite (HAP), and basic oxides as MgO [3–13].

Our preliminary studies [14] highlighted the key role of basic sites and high surface area of the catalyst to obtain better performance. In agreement with this finding, Birky et al. [15] proposed that strong basic sites facilitate the formation of butanol, presumably through a coupling reaction giving the aldol condensation, while inhibiting the C-C coupling reactions to C6 and heavier compounds that deactivates the catalyst at high temperature.

Chieregato et al. [16] reported that dehydrogenation is the first step of the Guerbet coupling over MgO forming a carbonyl intermediate. Díez et al. [17] proposed that, in the absence of metal promoters, ethanol dehydrogenation on basic metal oxides proceeds through an E1cB mechanism described as an initial dissociative adsorption of the alcohol on weak Lewis acid–strong Brönsted base pairs (Mg(A)–O) which break the OH bond forming a surface alkoxide intermediate [13].

In a recent paper [18], we demonstrated that dispersion of unpromoted or metal-promoted MgO on high surface area alumina pellets provided better results compared to the corresponding metal/MgO powder catalysts showing a lower surface area. The increase of surface area of MgO dispersed on γ-Al_2O_3 was also associated with a greater number of basic sites evaluated through CO_2 Temperature Programmed Desorption (TPD) tests.

All these results suggest that a higher dispersion of MgO and, consequently, a higher exposure of hydroxyl groups, can increase the number of sites activating the ethanol molecule thus improving conversion.

To this purpose, in this work, dispersion of MgO on a support with a larger surface area was proposed in order to further improve the catalytic performance. A cheap and easily available support, such as activated carbon (AC), was chosen to limit the costs of the overall process of production of butanol from bio-ethanol which also includes distillation of ABE mixture.

To the best of our knowledge, activated carbons have never been used for the Guerbet reaction whereas MgO dispersed on activated carbons has been proposed as sorbent for different gaseous species, such as CO_2 [19], H_2S [20,21], and organics [22,23] strongly increasing the adsorption capacity of the raw activated carbon.

Another issue related to the use of catalysts for Guerbet reaction is their possible deactivation in the presence of water. This represents an important concern for catalysts operating directly on the ABE mixture but also for systems proposed for the use downstream the separation of ethanol from the other components of the ABE mixture. Indeed, under real conditions, in order to limit costs, the azeotropic mixture (96% ethanol, 4% water) produced after distillation of ABE mixture can reasonably represent the feed. Zhu et al. [24] proposed a water-tolerant catalyst based on $Ni/MgO/SiO_2$ for ABE conversion into high-value bio-fuels as C_5-C_{15} ketones and alcohols due to the high stability of magnesium silicate structure compared to that of hydrotalcite, more commonly used for this reaction. Nevertheless, in all studies focused on the Guerbet reaction, the feed consisted of dry ethanol/inert gas mixture.

In this work, the effect of water on the catalytic performance in the Guerbet reaction of MgO supported on activated carbon has been also investigated and water resistance of this material compared to that of $Ru/MgO/\gamma$-Al_2O_3 catalyst previously tested under dry condition [18].

2. Materials and Methods

2.1. Preparation of Reference MgO and MgO/AC

Reference bulk MgO powder was obtained starting from Mg $(NO_3)_2$ $6H_2O$ (supplied by Sigma-Aldrich) aqueous solution by addition of ammonia solution with 5:1 NH_3:Mg ratio. The precipitate was stirred at 60 °C for 6 h in a closed bottle and, after filtration, dried at 120 °C overnight and calcined at 450 °C for 2 h, as described in Reference [14].

Aqueous solutions of $Mg(NO_3)_2$ $6H_2O$ were also used for the incipient wetness impregnation of acid washed granules of Darco G40 activated carbon (AC) (20 × 40 mesh, supplied by Cabot Norit Italia SpA) in order to obtain 10, 20, and 30 wt% MgO loadings, respectively. After drying at 120 °C in air, the catalysts were eventually calcined for 2 h at 600 °C under N_2.

A mechanical mixture consisting of 20 wt% MgO powder and 80 wt%. AC was also prepared to verify the effect of MgO dispersion onto the support. Finally, a $Ru/MgO/\gamma$-Al_2O_3 pellet catalyst prepared as described in Reference [18] was used as reference system for catalytic tests under both dry and wet feed conditions.

2.2. Characterization of MgO/AC Catalyst

Thermogravimetric (TG) analysis of the dried catalyst was performed in a Setaram Labsys Evo TGA-DTA-DSC 1600 flow microbalance loading about 30 mg sample in an alumina crucible and ramping the temperature at 10 °C/min up to 600 °C under pure N_2 (100 cc/min). The evolved gases flowed through a heated transfer line from TG balance to an infra-red (IR) cell of a Perkin Elmer Spectrum GX spectrometer.

XRD analysis was performed with a Bruker D2 Phaser diffractometer operated at diffraction angles ranging between 10° and 80° 2θ with a scan velocity equal to 0.02° 2θ s^{-1}.

Scanning electron microscopy (SEM) of cross-sectioned pellets was carried out with a FEI Inspect instrument equipped with an energy dispersive X-ray (EDX) probe.

Specific surface area and pore size distribution (PSD) were evaluated using a Quantachrome Autosorb 1-C by N_2 adsorption at 77 K after degassing samples for 2 h at 150 °C. The surface area was estimated according to the (Brunauer, Emmett, Teller) BET method whilst the PSD was evaluated according to the Non Localized Density Functional Theory (NLDFT) model.

2.3. Catalytic Tests

Catalytic tests were carried out in the temperature range 350–450 °C by feeding a 3 vol. % ethanol/N_2 mixture to a lab-scale fixed bed reactor of 0.3–1 g catalyst (corresponding to a gas hourly space velocity (GHSV) ranging between about 1000 and 300 h^{-1}), as described in Reference [18]. A main N_2 flow was bubbled through a liquid ethanol saturator at controlled temperature and the exit ethanol concentration was determined by the Antoine equation. An auxiliary flow of pure N_2 was used to dilute the main stream with such a ratio to obtain 3 vol.% ethanol in the total feed stream. The two gas streams were independently regulated by mass flow controllers. The reactor was operated at nearly atmospheric pressure, under pseudo-isothermal conditions. In some tests, the auxiliary nitrogen stream was pre-humidified by passing through a bubbler containing distilled water at room temperature. That allowed the introduction of about 2 vol.% H_2O to the inlet feed to the reactor. Reactants and products were analyzed by an online GC (Hewlett Packard 1540 A) equipped with FI detector and a ZB-WAX*plus* column. All species were separated except for ethylene from diethylether. GC peak areas were evaluated within 5% experimental error. Percentage butanol yield was expressed as butanol produced/ethanol reacted × 100 (vol./vol.)

3. Results and Discussion

3.1. Characterization of Fresh Catalysts

A preliminary TG analysis of 20% MgO/AC dried sample under N_2 up to 600 °C coupled to IR analysis of released gases indicated that nitrates decomposition was completed below 400 °C. Above this temperature, only a slow transformation of $Mg(OH)_2$ into MgO took place. Therefore, all catalysts treated at 600 °C consist of MgO dispersed on activated carbon without any residual presence of nitrate precursor salt.

Table 1 reports a list of catalysts together with their corresponding values of BET surface area and total pore volume. Upon dispersion of 10 wt% of MgO on the AC support, the original surface area was correspondingly reduced by ca. 10%. Further addition of MgO up to 20 wt% did not further modify both the surface area and pore volume; however, dispersion of 30% MgO induced a marked drop of about 37% of the original values of the parent carbon suggesting that some MgO aggregation takes place at high loadings, partially clogging pores, as also observed by Siriwardane et al. [20].

Table 1. BET (Brunauer, Emmett, Teller) surface area, total pore volume, and average crystallite size for MgO/AC supported catalysts.

Catalyst	BET Area (m^2/g)	Pore Volume (cm^3/g)	Average Crystallite Size (nm)
MgO powder	26	0.067	-
AC	641	0.81	-
10%MgO/AC	576	0.63	11.5
20%MgO/AC	578	0.61	22.3
30%MgO/AC	403	0.44	32.6

The pore size distribution (PSD) for raw AC and MgO/AC catalysts at different loadings are reported in Figure 1.

The parent activated carbon shows a tri-modal PSD with a large fraction of very small micropores (diameter < 7 Å), a fraction of micropores peaked at about 11 Å, and mesopores in the range 25–70 Å. The addition of 10 wt.% MgO results in a limited reduction of the large micropores, whereas the

addition of higher amounts of MgO (20 and 30 wt%) reduces both the fraction of very small micropores and that of mesopores. Furthermore, only for 20% MgO/AC, the amount of micropores with diameters around 11 Å increases. On the contrary, the massive formation of MgO aggregates occurring for 30% MgO loading leads to a significant occlusion of ultramicro- and meso-pores.

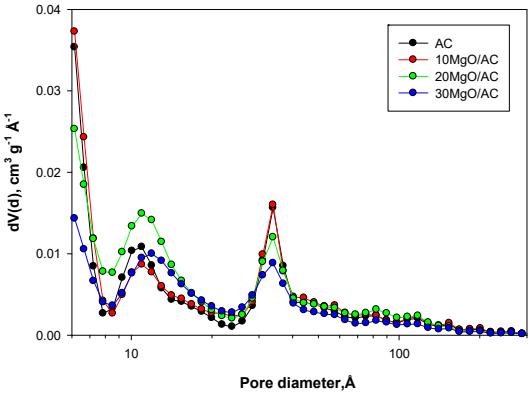

Figure 1. Pore size distribution (PSD) of activated carbon (AC) and of 10, 20, and 30 wt% MgO/AC.

The good dispersion of MgO onto active carbon was confirmed by SEM/EDX analysis performed on cross sections of the impregnated carbon granules: The EDS maps for Mg, reported in Figure 2 for the case 20% MgO/AC sample, clearly indicate that the impregnation procedure with magnesium nitrate solution guaranteed a uniform penetration of the precursor throughout the entire volume of the carbon particles having original characteristic dimensions in the range from 0.42 to 0.84 mm.

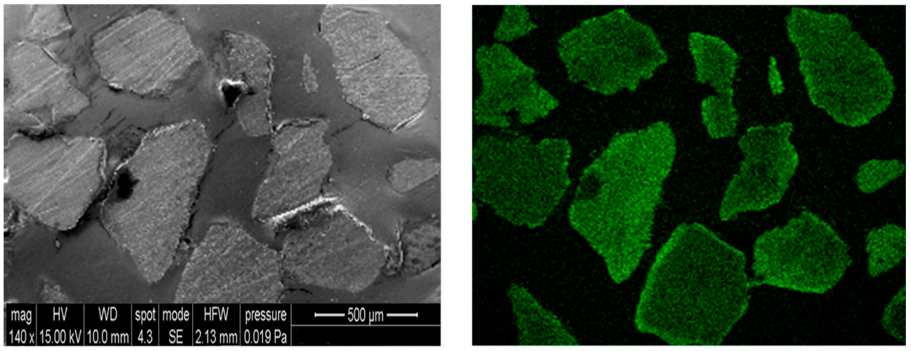

Figure 2. SEM image (left) and Mg EDX mapping (right) of 20% MgO/AC.

XRD patterns of AC and 10, 20, and 30 wt% MgO/AC are shown in Figure 3. Weak signals due to the characteristic reflections of MgO periclase (JCPDS 45-946) were found in the pattern of all MgO/AC samples, already for 10 wt% loading, in addition to the broad signals of the parent carbon support, which also contains some quartz impurities [25]. In contrast, Zhang et al. [21] did not detect MgO signals up to 20% MgO, most likely due to the much larger surface area of their activated carbon support. MgO signals become more intense by increasing the MgO content, indicating the formation of larger periclase crystallites. The average crystallite size, evaluated according to the Scherrer equation applied to the main MgO peak (42.8°) and reported in Table 1, progressively increases along with the MgO loading up to 32.3 nm for 30% MgO/AC. The significant occlusion of small micropores (<7 Å) detected for this sample confirms that most of the MgO is located outside of the micropore structure of the AC support.

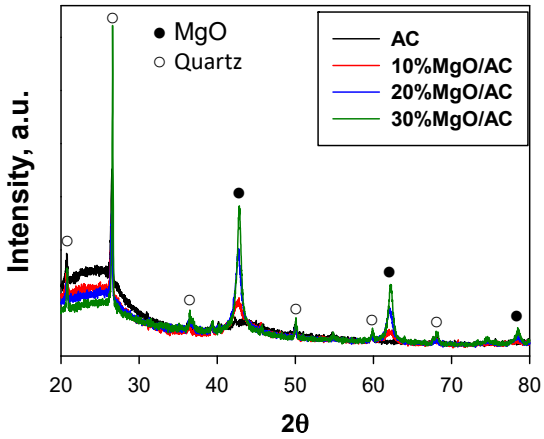

Figure 3. XRD patterns of raw AC and 10, 20, and 30 wt% MgO/AC.

3.2. Catalytic Tests

The effect of the GHSV was preliminarily explored at 400 °C on 20% MgO/AC sample by varying the catalyst load in the reactor while keeping unchanged the total flow rate and the inlet ethanol concentration. Results are reported in Figure 4 in terms of ethanol conversion and butanol yield. As expected, the ethanol conversion increases by reducing the GHSV, as also reported by Birky et al. [15]. Notably, also the process yield to butanol increases for lower values of the GHSV. It should be noticed that the largest amount of catalyst loaded in our experiments (1 g) corresponded to a catalytic bed height of about 3 cm; longer catalyst beds would have exceeded the isothermal zone of the electrical furnace and, therefore, lower values of the GHSV were not explored. On the other hand, a negligible butanol production was obtained performing tests at 350 °C even using the largest possible dose of catalyst.

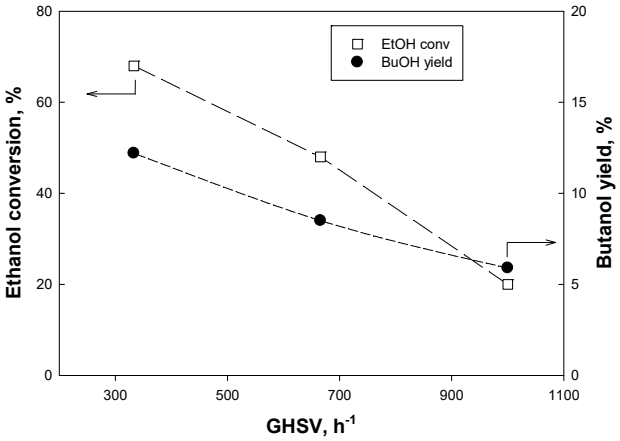

Figure 4. Ethanol conversion and butanol yield obtained in catalytic tests on 20% MgO/AC at 400 °C as a function of the gas hourly space velocity (GHSV).

All tests shown below were performed at GHSV 330 h^{-1}, that is the value providing the maximum ethanol conversion and butanol yield under isothermal conditions.

In Figure 5, the catalytic performance of MgO/AC systems with different loadings of the active phase are compared with results obtained over the bulk MgO catalyst under the same operating conditions. For all samples, in addition to butanol, the main product of the reaction was acetaldehyde. A lot of small and not identified peaks were also detected.

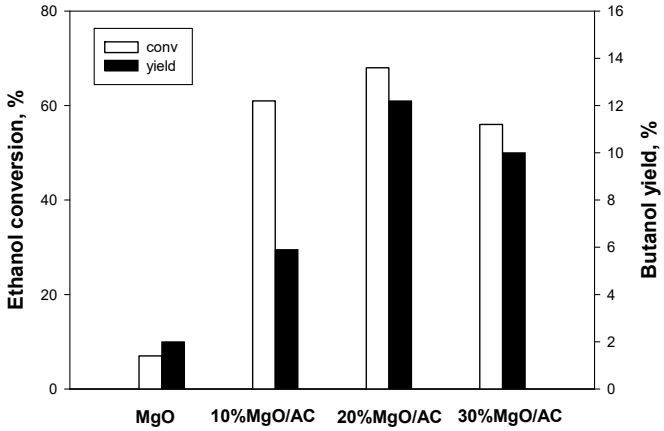

Figure 5. Ethanol conversion and butanol yield obtained in catalytic tests on pure MgO and AC supported MgO catalysts at T = 400 °C and GHSV = 330 h^{-1}.

Results reported in the figure highlight the key role of MgO dispersion. Indeed, the catalytic activity of bulk MgO is rather low, either in terms of ethanol conversion (<10%) and butanol yield (ca. 2%). However, when dispersed on the high surface area microporous activated carbon, the activity of the same MgO active phase is greatly enhanced, in spite of its lower content in the catalytic bed (only 10%–30% by weight). Best results were obtained with the catalysts containing 20 wt% MgO, which produced 12.5% butanol yield in correspondence of 68% ethanol conversion. For higher MgO contents, both conversion and yield decreased, most likely because of the formation of large MgO aggregates evidenced by reduction of both surface area and pore volume for 30% MgO/AC sample (Table 1).

A butanol yield at 350 °C similar to that obtained by us with 20% MgO/AC was reported by Carvalho et al. [11] for 3:1 Mg-Al mixed oxide (S.A. = 252 m^2/g) obtained by thermal decomposition of hydrotalcite. Nevertheless, experimental conditions are not easily comparable. On the other hand, a direct comparison with results obtained with 20 wt% MgO dispersed on γ-Al_2O_3 pellets [18], tested under the same reaction conditions, suggests that the enhancement in conversion and yield for the AC-supported sample is roughly proportional to the increase of surface area of this catalyst with respect to the alumina-supported one (S.A. = 115 m^2/g) having an identical loading of MgO.

Furthermore, in order to rule out a possible contribution of carbon to the reaction and to confirm the role of MgO dispersion, a mechanical mixture consisting in 20% MgO powder and 80% AC was also tested at 400 °C under the same space velocity. This sample provided an almost undetectable butanol yield further confirming the superior performance of highly dispersed MgO and excluding, at the same time, that the active carbon support has a direct catalytic activity for the Guerbet reaction.

Notably, butanol yields herein reported for all MgO/AC catalysts are significantly higher than those previously obtained on Ni/MgO/γ-Al_2O_3 pellets tested under the same experimental conditions [18]. In that case, the butanol yield was limited to 6%, in spite of the addition of the metal which was shown to promote the first step of the reaction mechanism.

All tests presented up to now were carried out under dry conditions, but water is generally present in the ethanol feed or it can be produced as a by-product, and it may cause irreversible or reversible catalyst deactivation. Therefore, in order to investigate those effects, some catalytic tests were repeated on the most-performing sample (20% MgO/AC) starting from dry feed conditions, then adding 2 vol % of H_2O for a total of 9 h on stream, and eventually switching back to a dry feed. The results of this sequence are reported in Figure 6.

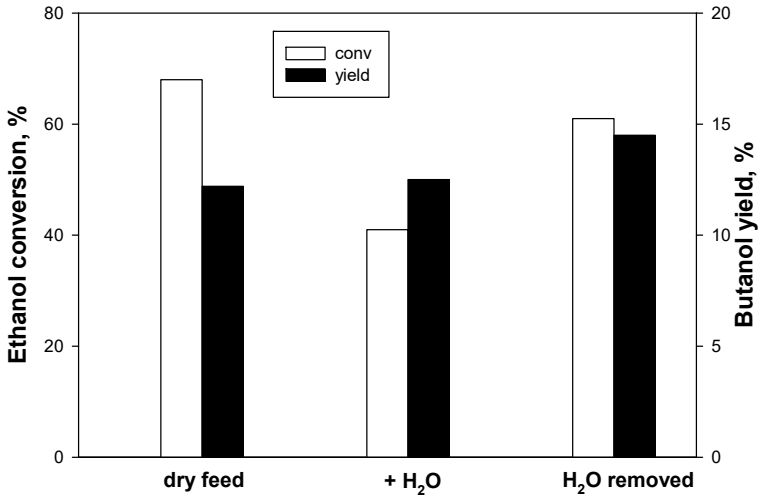

Figure 6. Effect of 2 vol. % H_2O addition to the feed (for a total of 9 h) and removal on the ethanol conversion and butanol yield obtained with a 20%MgO/AC sample tested at T = 400 °C and GHSV = 330 h^{-1}.

Notably, the addition of water induced a significant reduction of ethanol conversion from 68% down to ca. 40%, but the yield to butanol was not affected and remained around 12.5%. This implies that water is capable to enhance the process selectivity to butanol, suppressing some of the undesired side reactions consuming ethanol to form unidentified products, excluding acetaldehyde. The effluent stream from the catalytic reactor operated under wet feed conditions was monitored for a total of 9 h measuring a rather stable butanol production. Results in Figure 6 obtained after the removal of water from the feed indicated that its effects were not completely reversible: the ethanol conversion increased to ca. 61%, slightly below the initial level, but, most important, the yield to butanol increased up to 14.5%. This could be associated to an increase of the surface area that occurs when water weakly gasifies the activated carbon. Indeed, the surface area of the catalyst after the exposure to wet reaction conditions at 400 °C increased up to 750 m^2/g due to an evident increase of both kinds of micropores, as shown in Figure 7. This is in agreement with results reported by Gong et al. [26] who regulated the pore size distribution of their activated carbon through steam activation of coal containing different amount of potassium hydroxide. They found an optimal KOH fraction determining the maximum increase of micropores in the range 1–2 nm. The presence of water during the reaction with the consequent formation of basic $Mg(OH)_2$ could promote the large increase of micropores observed in the catalyst used under wet condition. Furthermore, the much higher solubility of magnesium hydroxide can promote some re-dispersion of the active phase thus leading to a catalyst with further enhanced properties compared with those attainable by the incipient wetness impregnation of AC. On the other hand, the total pore volume of the catalyst decreased down to 0.27 cm^3/g, mostly due to a marked loss of mesopores (Figure 7), which might be related to the deposition of some by-products of reaction.

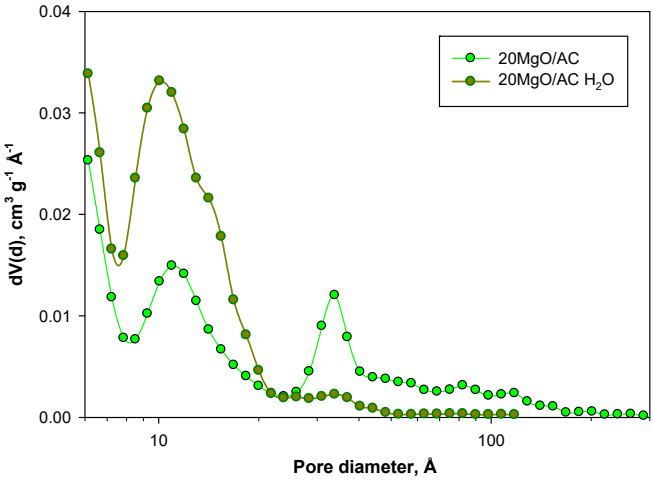

Figure 7. Effect of the exposure to wet reaction conditions at 400 °C for a total of 9 h on the PSD of a fresh 20% MgO/AC catalyst.

In order to highlight the key role of the activated carbon support in providing high water tolerance to supported MgO catalysts, the same sequence of experiments above described was performed on a Ru/MgO/γ-Al_2O_3 system reported in Reference [18] that achieved the best performance among a series of Me/MgO/γ-Al_2O_3 catalytic pellets. The experiments were carried out at 350 °C representing the best operating temperature for this material [18]. Results are shown in Figure 8 and clearly demonstrate that water addition induced a significant loss of activity for this catalyst and severely inhibited butanol production. In fact, both ethanol conversion and butanol yield dropped to less than 50% of their original value under dry feed conditions.

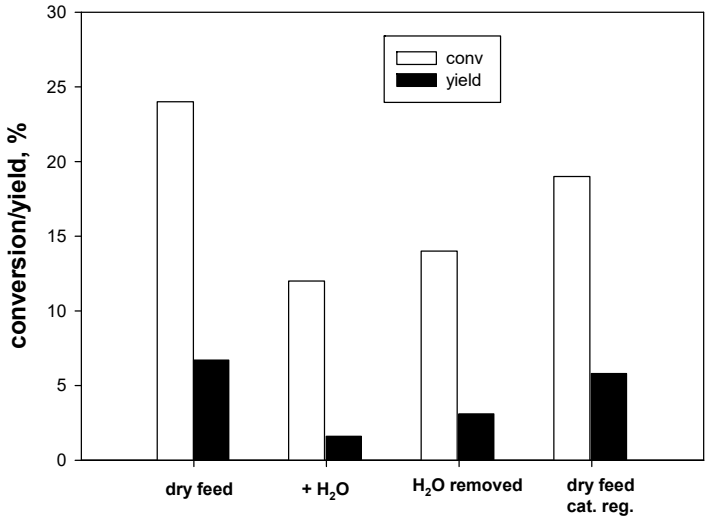

Figure 8. Effect of 2 vol. % H_2O addition to the feed (for a total of 9 h) and removal onto the ethanol conversion and butanol yield obtained with a Ru/MgO/γ-Al_2O_3 catalyst tested at T = 350 °C and GHSV = 330 h^{-1}. The fourth test was performed under dry conditions after catalyst regeneration for 2 h at 600 °C in air.

Upon H_2O removal, the recovery of catalytic performance with respect to the fresh catalyst was limited. Due to the inorganic nature of the alumina support material, it was possible to attempt to regenerate this catalyst via a thermal treatment at 600 °C for 2 h under an air flow. Thereafter, a reaction test under dry condition showed a further (not complete) recovery of the ethanol conversion while the butanol yield almost approached the initial level achieved by the fresh catalyst, suggesting that

deactivation by water was largely due to the irreversible deposition of some C-species masking the active phase.

In conclusion, this work demonstrates outstanding performance for the catalytic coupling of ethanol into butanol over MgO-based catalysts dispersed on activated carbons, not only under dry feed conditions but, particularly, in the presence of water. A direct comparison with the results obtained with more expensive $Ru/MgO/Al_2O_3$ catalysts highlights the key role of the activated carbon support to achieve a high water tolerance and an enhanced process selectivity towards butanol production. The development of such a new class of catalysts paves the way to operation with the azeotropic ethanol/water mixtures thus avoiding the need for a further purification step of ethanol, consequently lowering costs of the whole process of butanol production from ABE fermentation.

Author Contributions: Data curation, J.A.; investigation, S.C. and L.L.; supervision, L.L.; writing—original draft, L.L.; writing—review and editing, S.C.

Funding: This research was funded by the European Union's research and innovation program Horizon 2020. Waste2Fuels project 'Sustainable production of next generation biofuels from waste streams' (N. 654623).

Acknowledgments: Authors are grateful to Luciano Cortese (IRC-CNR) for SEM/EDX analysis and Giuseppe Mocci (University Federico II, Naples) for XRD analysis.

Conflicts of Interest: The authors declare no conflict of interest.

References

1. Patel, A.D.; Telalović, S.; Bitterb, J.H.; Worrell, E.; Patel, M.K. Analysis of sustainability metrics and application to the catalytic production of higher alcohols from ethanol. *Catal. Today* **2015**, *239*, 56–79. [CrossRef]
2. Earley, J.H.; Bourne, R.A.; Watson, M.J.; Poliakoff, M. Continuous catalytic upgrading of ethanol to *n*-butanol and $>C_4$ products over Cu/CeO_2 catalysts in supercritical CO_2. *Green Chem.* **2015**, *17*, 3018–3025. [CrossRef]
3. Ndou, A.S.; Plint, N.; Coville, N.J. Dimerisation of ethanol to butanol over solid-base catalysts. *Appl. Catal. A* **2003**, *251*, 337–345. [CrossRef]
4. Riittonen, T.; Toukoniitty, E.; Kumar Madnani, D.; Leino, A.R.; Kordas, K.; Szabo, M.; Sapi, A.; Arve, K.; Wärnå, J.; Mikkola, J.P. One-Pot Liquid-Phase Catalytic Conversion of Ethanol to 1-Butanol over Aluminium Oxide—The Effect of the Active Metal on the Selectivity. *Catalysts* **2012**, *2*, 68–84. [CrossRef]
5. Tsuchida, T.; Sakuma, S.; Takeguchia, T.; Ueda, W. Direct Synthesis of *n*-Butanol from Ethanol over Nonstoichiometric Hydroxyapatite. *Ind. Eng. Chem. Res.* **2006**, *45*, 8634–8642. [CrossRef]
6. Tsuchida, T.; Kuboa, J.; Yoshioka, T.; Sakuma, S.; Takeguchia, T.; Ueda, W. Reaction of ethanol over hydroxyapatite affected by Ca/P ratio of catalyst. *J. Catal.* **2008**, *259*, 183–189. [CrossRef]
7. Ogo, S.; Onda, A.; Yanagisawa, K. Selective synthesis of 1-butanol from ethanol over strontium phosphate hydroxyapatite catalysts. *Appl. Catal. A* **2011**, *402*, 188–195. [CrossRef]
8. Gines, J.L.M.; Iglesia, E. Bifunctional Condensation Reactions of Alcohols on Basic Oxides Modified by Copper and Potassium. *J. Catal.* **1998**, *176*, 155–172. [CrossRef]
9. Ueda, W.; Kuwabara, T.; Ohshida, T.; Morikawa, Y.A. A low-pressure Guerbet reaction over magnesium oxide catalyst. *J. Chem. Soc. Chem. Commun.* **1990**, 1558–1559. [CrossRef]
10. Marcu, I.-C.; Tichit, D.; Fajula, F.; Tanchoux, N. Catalytic valorization of bioethanol over Cu-Mg-Al mixed oxide catalysts. *Catal. Today* **2009**, *147*, 231–238. [CrossRef]
11. Carvalho, D.L.; de Avillez, R.R.; Rodrigues, M.-T.; Borges, L.E.; Appel, L.G. Mg and Al mixed oxides and the synthesis of n-butanol from ethanol. *Appl. Catal. A* **2012**, *415*, 96–100. [CrossRef]
12. Hanspal, S.; Young, Z.D.; Shou, H.; Davis, R.J. Multiproduct Steady-State Isotopic Transient Kinetic Analysis of the Ethanol Coupling Reaction over Hydroxyapatite and Magnesia. *ACS Catal.* **2015**, *5*, 1737–1746. [CrossRef]
13. Young, Z.D.; Davis, R.J. Hydrogen transfer reactions relevant to Guerbet coupling of alcohols over hydroxyapatite and magnesium oxide catalysts. *Catal. Sci. Technol.* **2018**, *8*, 1722–1729. [CrossRef]
14. Cimino, S.; Lisi, L.; Romanucci, S. Catalysts for conversion of ethanol to butanol: Effect of acid-base properties. *Catal. Today* **2018**, *304*, 58–63. [CrossRef]
15. Birky, T.W.; Kozlowski, J.T.; Davis, R.J. Isotopic transient analysis of the ethanol coupling reaction over magnesia. *J. Catal.* **2013**, *298*, 130–137. [CrossRef]

16. Chieregato, A.; Velasquez Ochoa, J.; Bandinelli, C.; Fornasari, G.; Cavani, F.; Mella, M. On the Chemistry of Ethanol on Basic Oxides: Revising Mechanisms and Intermediates in the Lebedev and Guerbet reactions. *ChemSusChem* **2015**, *8*, 377–388. [CrossRef] [PubMed]
17. Díez, V.K.; Apesteguía, C.R.; Di Cosimo, J.I. Acid–base properties and active site requirements for elimination reactions on alkali-promoted MgO catalysts. *Catal. Today* **2000**, *63*, 53–62. [CrossRef]
18. Apuzzo, J.; Cimino, S.; Lisi, L. Ni or Ru supported on MgO/γ-Al_2O_3 pellets for the catalytic conversion of ethanol into butanol. *RCS Adv.* **2018**, *8*, 25846–25855. [CrossRef]
19. Shahkarami, S.; Dalai, A.K.; Soltan, J. Enhanced CO_2 Adsorption Using MgO-Impregnated Activated Carbon: Impact of Preparation Techniques. *Ind. Eng. Chem. Res.* **2016**, *55*, 5955–5964. [CrossRef]
20. Siriwardane, I.W.; Udangawa, R.; de Silva, R.M.; Kumarasinghe, A.R.; Acres, R.G.; Hettiarachchi, A.; Amaratunga, G.A.J.; de Silva, K.M.N. Synthesis and characterization of nano magnesium oxide impregnated granular activated carbon composite for H_2S removal applications. *Mater. Des.* **2017**, *136*, 127–136. [CrossRef]
21. Zhang, Z.; Wang, J.; Li, W.; Wang, M.; Qiao, W.; Long, D. Millimeter-sized mesoporous carbon spheres for highly efficient catalytic oxidation of hydrogen sulfide at room temperature. *Carbon* **2016**, *96*, 608–615. [CrossRef]
22. Rezaei, F.; Moussavi, G.; Bakhtiari, A.R.; Yamini, Y. Toluene removal from waste air stream by the catalytic ozonation process with MgO/GAC composite as catalyst. *J. Hazard. Mater.* **2016**, *306*, 348–358. [CrossRef] [PubMed]
23. Zhou, K.; Li, L.; Ma, X.; Mo, Y.; Chen, R.; Li, H.; Li, H. Activated carbons modified by magnesium oxide as highly efficient sorbents for acetone. *RSC Adv.* **2018**, *8*, 2922. [CrossRef]
24. Zhu, Q.; Shen, C.; Wang, J.; Tan, T. Upgrade of Solvent-Free Acetone−Butanol−Ethanol Mixture to High-Value Biofuels over Ni-Containing MgO−SiO_2 Catalysts with Greatly Improved Water-Resistance. *ACS Sustain. Chem. Eng.* **2017**, *5*, 8181–8191. [CrossRef]
25. Balsamo, M.; Cimino, S.; de Falco, G.; Erto, A.; Lisi, L. ZnO-CuO supported on activated carbon for H_2S removal at room temperature. *Chem. Eng. J.* **2016**, *304*, 399–407. [CrossRef]
26. Gong, G.-Z.; Xie, Q.; Zheng, Y.-F.; Ye, S.-F.; Chen, Y.-F. Regulation of pore size distribution in cola based activated carbon. *New Carbon Mater.* **2009**, *24*, 141–146. [CrossRef]

© 2019 by the authors. Licensee MDPI, Basel, Switzerland. This article is an open access article distributed under the terms and conditions of the Creative Commons Attribution (CC BY) license (http://creativecommons.org/licenses/by/4.0/).